

# Global mass segregation in hydrodynamical simulations of star formation

Th. Maschberger<sup>1,2,3\*</sup> & C.J. Clarke<sup>3</sup>

<sup>1</sup> *Institut de Planétologie et d'Astrophysique de Grenoble, BP 53, F-38041 Grenoble Cédex 9, France*

<sup>2</sup> *Argelander-Institut für Astronomie, Auf dem Hügel 71, D-53121 Bonn, Germany*

<sup>3</sup> *Institute of Astronomy, Madingley Road, Cambridge CB3 0HA, England*

MNRAS accepted

## ABSTRACT

Recent analyses of mass segregation diagnostics in star forming regions invite a comparison with the output of hydrodynamic simulations of star formation. In this work we investigate the state of mass segregation of ‘stars’ (i.e. sink particles in the simulations) in the case of hydrodynamical simulations which omit feedback. We first discuss methods to quantify mass segregation in substructured regions, either based on the minimum spanning tree (Allison’s  $\Lambda$ ), or through analysis of correlations between stellar mass and local stellar surface number densities. We find that the presence of even a single ‘outlier’ (i.e. a massive object far from other stars) can cause the Allison  $\Lambda$  method to describe the system as inversely mass segregated, even where in reality the most massive sink particles are overwhelmingly in the centres of the subclusters. We demonstrate that a variant of the  $\Lambda$  method is less susceptible to this tendency but also argue for an alternative representation of the data in the plane of stellar mass versus local surface number density.

The hydrodynamical simulations show global mass segregation from very early times which continues throughout the simulation, being only mildly influenced during sub-cluster merging.

We find that up to  $\approx 2\text{--}3\%$  of the “massive” sink particles ( $m > 2.5 M_{\odot}$ ) are in relative isolation because they have formed there, although other sink particles can form later in their vicinity. Ejections of massive sinks from subclusters do not contribute to the number of isolated massive sink particles, as the gravitational softening in the calculation suppresses this process.

**Key words:** stars: formation – open clusters and associations: general – methods: data analysis

## 1 INTRODUCTION

The relative spatial distributions of stars of different masses can give valuable insights into the evolution of young star forming regions. Traditionally, what is termed ‘mass segregation’ (i.e. the concentration of more massive stars within dense cluster cores) has been interpreted as a stellar dynamical effect (i.e. the result of two-body relaxation), although there are apparently cases where the system is so young that the central concentration of massive stars must be primordial (Bonnell & Davies 1998). More recently, hydrodynamical simulations of star formation in turbulent molecular clouds have illustrated the bottom-up creation of star clusters through sub-cluster merging, which rather blunts the distinction between primordial and dynamical mass segregation (see e.g. Allison et al. 2009a and Allison et al. 2010 for purely stellar-dynamical aspects of primordial vs. dynamical mass segregation). What has

now become important is instead to assess the realism of such simulations by comparing their mass segregation characteristics with those of observed star forming regions. With this in mind it is important to develop robust and flexible diagnostics that can be applied to simulations and observations alike.

Currently there are a variety of claims in the literature about the degree of mass segregation in star forming regions: Parker et al. (2011) find “inverse” mass segregation for Taurus, implying that massive stars are more widely distributed than average and found preferentially isolated compared to intermediate-mass stars. On the other hand Kirk & Myers (2011) find a concentration of massive stars in the centres of groups in Taurus, Lupus3, ChaI, and IC348; Schmeja et al. (2008) report no signs of mass segregation for NGC1333 and L1688, but find that the older regions IC348 and Serpens are mass segregated. Mass segregation has also been reported for more massive young star clusters like the ONC (Hillenbrand & Hartmann 1998; Allison et al. 2009b), NGC3603 (Stolte et al. 2006) or NGC2244 (Chen et al. 2007) though Wang et al.

\* e-mail: thomas.maschberger@obs.ujf-grenoble.fr

(2008) find the latter not to be mass segregated. (See however Asencio et al. 2009 for a discussion of how incompleteness may affect these conclusions).

The association of stars with gas filaments in young star forming regions (see e.g. the recent Herschel results for Aquila Könyves et al. 2010; Bontemps et al. 2010; André et al. 2010) illustrates that *pure*  $n$ -body simulations are not sufficient to describe the dynamical evolution of these regions. Larger-scale hydrodynamical simulations of star cluster formation have been performed e.g. by Bonnell et al. (2003, 2008) or Bate (2009). Bate (2009) reported no evidence for mass segregation in his simulations, when analysed using cumulative radial fractions in different stellar mass ranges, but the analysis of Moeckel & Bonnell (2009) (using convex hulls) found that the most massive stars were indeed segregated, at a level comparable to that observed in the Orion Nebula Cluster. In this work we analyse the global mass segregation in the simulations of Bonnell et al. (2003) and Bonnell et al. (2008). This extends the analysis of Maschberger et al. (2010), where we have already studied mass segregation on a subcluster-by-subcluster scale.

For the analysis of mass segregation in a star forming region it is necessary to use a method that does not rely on spherical symmetry, as significant amounts of substructure can still be present. Additionally, the method should be able to detect a concentration of only the most massive stars, of which typically only a small number exists. Allison et al. (2009b) presented a method that is able to cope with both substructure and small numbers, (the  $\Lambda$  measure) and Parker et al. (2011) used this method to show that the massive stars in the Taurus star forming region are *inversely mass segregated*. This is somewhat in contrast to the result of Kirk & Myers (2011), who also analysed the Taurus region (albeit a different observational sample) and came to the opposite conclusion, namely mass segregation of the massive stars. However, Kirk & Myers (2011) analysed individual subclusters of stars in Taurus using the radial distance of the massive stars to the geometrical centre of the subcluster. Because of the different methods employed, it is not clear whether the Kirk & Myers (2011) result of local mass segregation may be directly compared to the Parker et al. (2011) result of global inverse mass segregation.

In our previous analysis of star formation simulations (Maschberger et al. 2010) we followed both methodologies: i.e. the approach of Kirk & Myers (2011), using radial distances for lower- $n$  subclusters, and the approach of Parker et al. (2011), using the  $\Lambda$  measure for sufficiently populous subclusters. We found that generally mass segregation prevails *within subclusters* at all times apart from the very earliest stages of their formation. Again, our result is not directly comparable to Parker et al. (2011), because we have not analysed the simulation as a whole, but individual subclusters.

Therefore in this work we analyse the simulations of Bonnell et al. (2003) and Bonnell et al. (2008) in the same manner as Parker et al. (2011) in order to assess whether the simulations produce stellar distributions that are compatible with those observed throughout the Taurus star forming region. During the analysis we found that the  $\Lambda$  method can produce misleading results when a small number of high-mass stars are present in low-density regions and that this might be the reason for the different results of Parker et al. (2011) and Kirk & Myers (2011). In order to address this shortcoming we suggest a modification to the  $\Lambda$  method that is less sensitive to a small number of massive outliers. We also point out that plots of stellar mass as a function of surface density provide a ready way to compare the output of simulations with observations. Such plots provide helpful visualisation in arbitrary geometry and allow one to easily spot and assess the presence of isolated high-mass stars.

The outline of this paper is as follows: We first describe the hydrodynamical simulations (Section 2). In the following section we describe the  $\Lambda$  method to quantify mass segregation in substructured data. Section 4 describes the state of mass segregation in the simulations when analysed in terms of local stellar densities. We finish with a summary and discussion in Section 5.

## 2 HYDRODYNAMICAL SIMULATIONS

The data for our analysis are from the smoothed particle hydrodynamics (SPH) simulations by Bonnell et al. (2003) and Bonnell et al. (2008), as also analysed in Maschberger et al. (2010). In these cited works one can find detailed descriptions of the setup of the calculations and their evolution.

Bonnell et al. (2003) followed the self-gravitating evolution of a gas sphere containing  $1000 M_{\odot}$  gas in a diameter of 1 pc with a temperature of 10 K, which is initially marginally unbound. An initial divergence-free random Gaussian velocity with a power spectrum  $P(k) \propto k^{-4}$  models initial turbulent motions. The gas is kept isothermal throughout the calculation and feedback is not included. Sink particles replace dense regions when a critical density of  $1.5 \times 10^{-15} \text{ g cm}^{-3}$  is exceeded, and can continue to accrete either if a gas particle becomes gravitationally bound within a sink radius of 200 au or if a gas particle moves within the accretion radius of 40 au. The mass resolution is  $\approx 0.1 M_{\odot}$ , and gravitational forces between sinks are smoothed at 160 au. In this simulation one final “star cluster” is formed at the end of the simulation time, at  $\approx 4.8 \times 10^5 \text{ yr}$  or  $\approx 2.5$  initial free-fall times, and it contains  $\approx 560$  sink particles with  $m > 0.08 M_{\odot}$ .

The simulation of Bonnell et al. (2008) starts with a gas mass of  $10^4 M_{\odot}$ , arranged in a cylinder having 10 pc length and 3 pc diameter with a linear density gradient along the main axis (33 % higher density than average on one end, 33 % lower on the other). The initial turbulence is modelled as in the  $10^3 M_{\odot}$  calculation, but the gas follows a barotropic equation of state during the simulation. Again this simulation does not include feedback effects, and star formation is modelled via sink particles, with a critical density of  $6.8 \times 10^{-14} \text{ g cm}^{-3}$ , a sink radius of 200 au and an accretion radius of 40 au. The gravitational softening length is 40 au. At the end, after  $\approx 6.5 \times 10^5 \text{ yr}$  or  $\approx 1$  initial free fall time,  $\approx 1900$  sink particles are formed ( $m > 0.08 M_{\odot}$ ). The spatial distribution of the sink particles is still substructured, with several larger clusters and a population along filaments.

## 3 MEASURING MASS SEGREGATION USING MINIMUM SPANNING TREES

### 3.1 Method

The basis for calculating  $\Lambda$  of Allison et al. (2009b) is the minimum spanning tree (MST), a graph-theoretical concept, which is the unique connection of a set of points such that there are no closed loops and with the property that the total length of the connections (edges) is minimal. Algorithms to calculate the MST, further properties, and some applications of the MST to analyse the structure in spatial data can be found in Zahn (1971). A schematic sketch illustrating how  $\Lambda$  works is given in Figure 1, showing the spatial distribution of a mass segregated region, with dots for low-mass stars and stars for high-mass stars. To obtain  $\Lambda$ , calculate first the MST of the six most massive stars of a star cluster, shown with the solid lines in Fig. 1. Denote the average edge length of this MST with

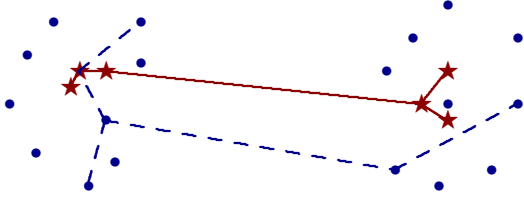


**Figure 1.** Sketch illustrating the ability of MST methods to detect mass segregation in substructured regions. Stars indicate the position of massive stars, with their MST shown as solid lines, and points the location of low-mass stars. An MST of six random stars is shown with dashed lines. Typically, a random set of six stars contains stars from both subclusters. Therefore, both the MST for massive and random stars contain the long connection between the two subclusters, which averages out when they are compared.

$\bar{l}_{\text{massive}}$ . Consider now the MST of a set of six stars that are randomly taken from the star cluster (e.g. the dashed lines in Fig. 1), with average edge length  $\bar{l}_{\text{random}}$ . The MST of one particular random set of six stars contains not much information, but the sample average of the average length,  $\bar{l}_{\text{random}}$ , calculated from a number of sets containing six randomly drawn stars, characterises the spatial distribution of stars in the star cluster. To quantify mass segregation one now compares  $\bar{l}_{\text{massive}}$  with  $\bar{l}_{\text{random}}$ . Mass segregation is commonly understood as a more central concentration of the massive stars compared to all stars of the star cluster or, more generally, a more compact configuration of the massive stars. Therefore, in a mass segregated cluster, the massive stars will have a much shorter average MST edge length than random stars, i.e. if  $\bar{l}_{\text{massive}} < \bar{l}_{\text{random}}$  then the cluster is mass segregated. The statistical significance of this comparison can be expressed in standard deviations of  $\bar{l}_{\text{random}}$ .

The sketch of Fig. 1 shows a substructured region (or, rather, two subclusters), to illustrate the ability of  $\bar{\Lambda}$  to deal with substructure. The massive stars reside in the centres of the subclusters. Their MST contains four short edges (combining the stars within the subclusters) and one long edge, that connects the two subclusters. Similarly, an MST of six random stars will contain typically stars from both subclusters, so that the random MST contains some medium-length edges plus the long connection between the subclusters. Therefore,  $\bar{l}_{\text{massive}} = (\text{short} + \text{connection})/6$  is still smaller than  $\bar{l}_{\text{random}} = (\text{medium} + \text{connection})/6$ , even in the presence of substructure.

For the definition of the mass segregation measure we follow (Parker et al. 2011) by calculating  $\bar{\Lambda}$  within a sequence of different mass ranges (instead of calculating a measure for all stars from the most massive down to the  $i$ -th most massive star, as in Allison et al. (2009b)). The length of 40 stars for the moving window follows the choice of (Parker et al. 2011). We denote the Allison et al./Parker et al. measure with  $\bar{\Lambda}$  to indicate that it has been calculated with the average MST length.  $\bar{\Lambda}$  is derived from the mass-sorted sample of stars ( $m_{(1)} > m_{(2)} \dots$ ) for the  $i$ -th to the  $i+40$ -th most massive star according to

$$\bar{\Lambda}_{(i)}(\bar{m}_{(i)}) = \frac{\bar{l}_{40}}{\bar{l}_{(i),(i+40)}} \quad (1)$$

where  $\bar{m}_{(i)}$  is the average mass of the stars from the  $i$ -th to the  $i+40$ -th most massive star,  $\bar{l}_{40}$  is the sample average MST edge length of 40 random stars ( $\bar{l}_{\text{random}}$ ), and  $\bar{l}_{(i),(i+40)}$  is the average edge length of the MST containing the  $i$ -th to the  $i+40$ -th most

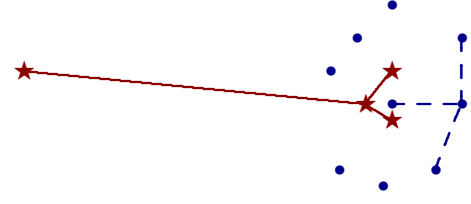


**Figure 2.** Sketch illustrating the difficulty of MST methods in the presence of outliers, like Fig. 1, showing the locations of massive stars with star symbols and their MST as solid lines. Here the MST for random stars (one example with dashed lines) only rarely contains the long distance to the outlying massive star. Thus, the random MST edge length is shorter on average compared to the massive star MST edge length, so that  $\bar{\Lambda}$  gives the result “inversely mass segregated”, although still most of the massive stars are in the centre of the cluster.

massive star ( $\bar{l}_{\text{massive}}$ ). The stars in the mass window are statistically significantly mass segregated if they fulfill

$$\bar{\Lambda}_{(i)}(\bar{m}_{(i)}) - \frac{\bar{\sigma}_{40}}{\bar{l}_{(i),(i+40)}} > 1, \quad (2)$$

where  $\bar{\sigma}_{40}$  is the standard deviation of  $\bar{l}_{40}$ .

In order to be less influenced by outliers we propose an analogous measure,  $\tilde{\Lambda}$ , that uses the median MST edge length instead of the mean. The equation for  $\tilde{\Lambda}$  reads then

$$\tilde{\Lambda}_{(i)}(\bar{m}_{(i)}) = \frac{\tilde{l}_{40}}{\tilde{l}_{(i),(i+40)}}, \quad (3)$$

with  $\tilde{l}_{(i),(i+40)}$  being the median edge length of the MST for the massive stars.  $\tilde{l}_{40}$  is the sample average of the median edge length of 40 random stars. The condition for statistically significant mass segregation is analogous to eq. 2, using  $\tilde{\sigma}_{40}$ , the standard deviation of  $\tilde{l}_{40}$ .

### 3.2 Inverse mass segregation indicated by $\bar{\Lambda}$

At early times of the 1000  $M_{\odot}$  simulation  $\bar{\Lambda}$  is smaller than unity, suggesting *inverse mass segregation*. Here we show that this result is strongly driven by a single massive outlier. The situation is illustrated schematically in Fig. 2, showing a mass segregated cluster with one massive outlier. Within the cluster, the MST of the massive stars (solid lines) has short edges, shorter than the medium length edges of a random MST (dashed). Without the isolated star, the  $\bar{\Lambda}$  method would demonstrate that the cluster is mass segregated; however when the single isolated massive star is included in the computation of  $\bar{\Lambda}_{\text{massive}}$ , the system would instead be classified as “inversely mass segregated”.

A concrete example from the 1000  $M_{\odot}$  simulation is given in Fig. 3, showing a snapshot of the sink particle distribution at an age of  $3 \times 10^5$  yr. At this time 413 sink particles with masses  $> 0.08 M_{\odot}$  have been formed. Sinks with  $m > 1 M_{\odot}$  are shown with larger dots, which are generally associated with subclusters. The big star marks the position of the outlier, a sink that has at this time a mass of  $4.2 M_{\odot}$  (the 16th most massive sink). The results for  $\bar{\Lambda}$  are given by the solid line in the upper panel of Fig. 4.  $\bar{\Lambda} < 1$  for  $m > 1 M_{\odot}$ , i.e. inverse mass segregation (although there is a “bump” around  $2 M_{\odot}$ ). The standard deviation of  $\bar{\Lambda}$  is 0.16, so that this result is not statistically significant. But, when the outlier is

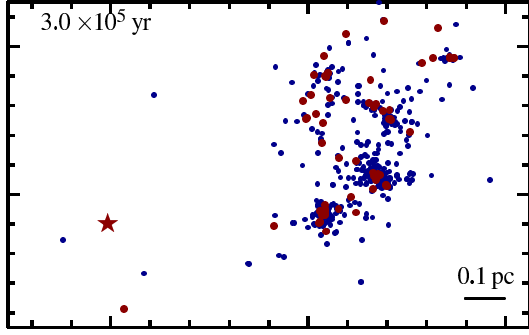


**Figure 3.** Projected positions of the sink particles in the 1000  $M_{\odot}$  simulation at a time of 300 000 yr, when 413 sink particles have been formed ( $m > 0.08 M_{\odot}$ ). Sink particles with a mass larger than 1 Msun are marked by the larger dots. The star marks the position of a rather massive sink particle ( $4.2 M_{\odot}$ ), that has formed earlier on at this fairly isolated location and continued to accrete.

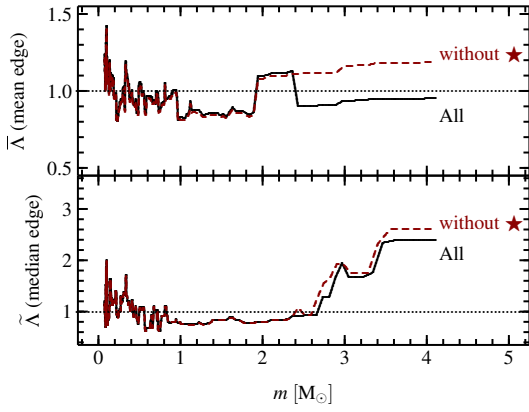


**Figure 4.**  $\bar{\Lambda}$  (top) and  $\tilde{\Lambda}$  calculated for the snapshot shown in Fig. 3, using all sink particles (solid lines) and excluding the isolated massive sink marked by a star in Fig. 3 (dashed lines). Removing the edge to the isolated massive sink changes the result of  $\bar{\Lambda}$  from “inversely mass segregated” to “mass segregated”.  $\tilde{\Lambda}$  is more robust to the removal of the isolated massive sink and shows only minor changes. Note that the absolute values of  $\bar{\Lambda}$  and  $\tilde{\Lambda}$  are not directly comparable.

removed, then  $\bar{\Lambda} \approx 1.2$  for  $m > 2 M_{\odot}$  (dashed line in the upper panel of Fig. 4), i.e. now the region is mass segregated.

The use of the median instead of the mean when calculating  $\Lambda$  leads to more robust results with respect to outliers. In the lower panel of Fig. 4  $\tilde{\Lambda}$  is shown, either including the outlier (solid line) or omitting it (dashed line). Both cases lead to the essentially identical curves, indicating that the sinks with  $m > 2.5 M_{\odot}$  are mass segregated. (The standard deviation of  $\tilde{\Lambda}$  is  $\approx 0.4$ ). It should be noted that the absolute values of  $\bar{\Lambda}$  and  $\tilde{\Lambda}$  are not directly comparable, i.e., omitting the outlier,  $\bar{\Lambda} = 1.2$  does *not* imply “less” mass segregation than  $\tilde{\Lambda} = 2$ ).

The above results demonstrate the obvious point that a single measure cannot contain all the information about the system - i.e. there is no value of either  $\bar{\Lambda}$  or  $\tilde{\Lambda}$  that uniquely demonstrates the actual situation shown in Figure 3 (i.e. a generally mass segregated situation plus a single massive outlier). In the following section we instead present plots of stellar mass versus surface density which can be readily compared with observations.

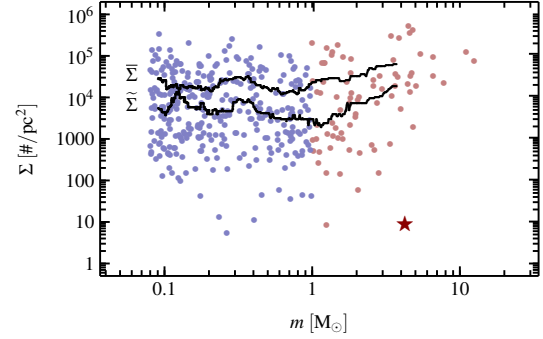


**Figure 5.** Stellar surface density vs. mass, calculated for the snapshot shown in Fig. 3. Also shown is the moving window mean ( $\bar{\Sigma}$ ) and median ( $\tilde{\Sigma}$ ) surface density (window size 40 sinks). The star marks the position of the outlier in Figure 3.

#### 4 MEASURING MASS SEGREGATION WITH STELLAR SURFACE DENSITIES

In the previous Section we discussed the advantage of utilising the MST to quantify mass segregation in substructured regions, but also the fact that the resulting statistic is very sensitive to outliers, especially when the mean edge length is used. Here we present as an alternative the use of a plot of stellar surface densities versus stellar mass, which can be also used in the presence of substructure. It allows one to have an immediate grasp of the state of mass segregation and the presence of outliers.

For the evaluation of the local surface number density around a star we follow the approach of von Hoerner (1963) and Casertano & Hut (1985). As we analyse the data in projection, we define for a star the local surface number density as

$$\Sigma = \frac{6 - 1}{\pi r_6^2}, \quad (4)$$

where  $r_6$  is the distance to the sixth nearest neighbour of the star. In the choice of the sixth nearest neighbour we follow Casertano & Hut (1985), who found that for a total number of particles between 30–1000 this choice is a good compromise between locality of the density estimate and the amount of low-number fluctuations.

Figure 5 gives an example of a plot of stellar density versus the sink particle mass for the snapshot of the 1000  $M_{\odot}$  simulation shown in Figure 3. The dots show the local estimates for each sink particle, spanning five orders of magnitude. It can immediately be seen that, whereas low mass sinks are found at all surface densities, there are few massive sinks in regions of low surface density. It is this relative deficit of points in the lower right of the plot that drives the correlation between mass and surface density as is evidenced by the rise in both median and mean mass with surface density at masses  $> 1 M_{\odot}$ . Note that the inclusion or omission of the “isolated” massive sink (marked with a star, as in Figure 3) would have little effect on the median and mean trends. Thus the plot allows one to readily discern the outliers without allowing them to dominate the inferences drawn about the distribution. The differences in the surface densities of low- and high-mass sinks can be more formally quantified by a two-sample Kolmogorov-Smirnov test. For this we divide the data shown in Fig. 5 into a low-mass sample ( $0.08 M_{\odot} < m \leq 1 M_{\odot}$ ,  $n = 334$ ) and a high-mass sample ( $m > 1 M_{\odot}$ ,  $n = 79$ ). The probability for those samples to obey the same distribution function is only 2.5% (p-value = 0.025), i.e., the

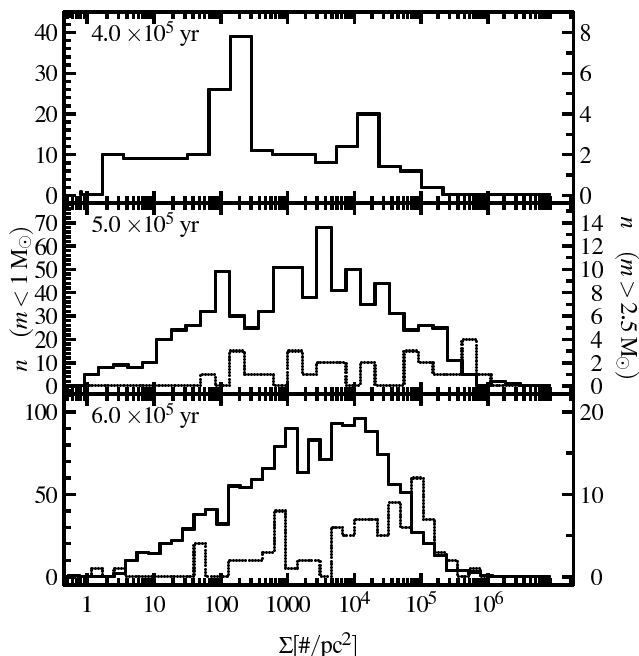


**Figure 6.** Histograms of the surface density of sink particles of the  $10^4 M_\odot$  simulation in the mass ranges  $0.08\text{--}2.5 M_\odot$  (solid) and  $> 2.5 M_\odot$  (dotted, right y axis scaled to 5 times the values for the lower range, as less sink particles have high masses). The first sink particle formed at  $3.2 \times 10^5$  yr. The lower mass sink particles move to higher surface densities, as the subclusters contract, but mergers of subclusters mean that some sinks continue to be found at low surface densities. Massive sink particles have generally higher surface densities, although some can be found at low surface densities because they formed in isolation.

surface density distribution of the more massive sinks is more than  $2\sigma$  deviating from the one of low-mass sinks.

Figure 6 shows a time sequence for the evolution of the surface density as a function of stellar mass, in this case in the case of the  $10^4 M_\odot$  simulation which forms a number of clusters (see Figure 2 of Maschberger et al. 2010 for the spatial distribution of the sinks). Evidently a large range of surface densities is present in each snapshot, with the low density tail being contributed both by regions of newly formed sinks together with clusters whose density has been temporarily lowered during mergers. The maximum surface density however increases over the period  $4 \times 10^5\text{--}6 \times 10^5$  yr as clusters merge and contract. As more massive sink particles ( $> 2.5 M_\odot$ ) are formed, they tend to populate the higher end of the surface density distribution (see dotted histograms in lower two panels). The two-sample KS probabilities are 0.8% at  $5 \times 10^5$  yr and  $6 \times 10^{-9}$  at  $6 \times 10^5$  yr, dividing the sample at  $2.5 M_\odot$ .

Note that even the more massive sink particles are occasionally found at low surface densities, as evidenced by the tail in the bottom panel of Fig. 6. For example, there are two massive sink particles ( $m = 2.8 M_\odot$  and  $m = 2.6 M_\odot$ ) with very low surface densities at  $6 \times 10^5$  yr (see lowest panel of Figure 6). They have formed and grown in relative isolation (one in the unbound part and the other in an outward-moving filament of the bound part of the cloud) and at the moment of the snapshot no other sink particle has formed nearby. In the time until the end of the simulation, some 50000 years later, a few sink particles form in the vicinity of both massive sinks, which themselves might in nature fragment to a binary or multiple system.

## 5 SUMMARY AND DISCUSSION

Hydrodynamical simulations of star forming regions (Bonnell et al. 2003, 2008; Maschberger et al. 2010) show a general trend of mass segregation within the first few 100 000 years. This follows with both using the minimum spanning tree technique (Λ, Allison et al. 2009b) and the distribution of local sink particle densities vs. mass. We note that the MST technique using the mean edge length, as suggested by Allison et al. (2009b), can give results that can be dominated by the presence of even a single star that in relative isolation from the main region. We suggest that using the median MST edge length (instead of the mean) is more robust against such outliers. The combined usage of mean and median indicates the trend for mass segregation of the majority of the massive stars as well as the presence of outliers.

Alternatively, it proves useful to study mass segregation with the  $m\text{--}\Sigma$  plot (mass vs. stellar surface number density), which can be applied in substructured regions and makes the presence of massive outliers immediately perceptible.

The observational results for Taurus, showing inverse Λ mass segregation (Parker et al. 2011) and a concentration of massive stars at subcluster centres with some “isolated” massive stars (Kirk & Myers 2011) may be compatible with the simulations. Although Taurus is a much sparser system than the one modelled here, it would be interesting to see whether the distribution of sources in the  $m\text{--}\Sigma$  plane is qualitatively similar to the simulations

In the simulations, “massive” sink particles ( $m > 2.5 M_\odot$ ) can form and stay for extended periods in relative isolation (stellar surface density  $< 10/\text{pc}^2$ , i.e.  $< 10^{-4}$  of the median surface density in the simulation). However, they are a small minority of only up to  $\approx 2\text{--}3\%$  of all massive sinks (1 of 33 in the  $1000 M_\odot$  calculation at  $t = 3 \times 10^5$  yr, 2 of 98 in the  $10^4 M_\odot$  calculation,  $t = 6 \times 10^5$  yr).

The softened gravitational potential hinders strong dynamical interactions of sink particles in the calculations and so also ejections of massive sinks. Therefore the occurrence of isolated massive sinks via the dynamical channel is possibly underestimated. Thus the figure of 2–3% represents the fraction of massive sinks that are relatively isolated and have formed in situ in the simulations. We cannot at present quantify the numbers of ejected massive sinks that might additionally appear in isolation.

## 6 ACKNOWLEDGEMENTS

Th. M. acknowledges funding through CONSTELLATION, an European Commission FP6 Marie Curie Research Training Network, and the Stellar Populations and Dynamics Research Group at the Argelander-Institut für Astronomie. We would like to thank Pavel Kroupa and Andreas Küpper for helpful comments regarding the manuscript.

## REFERENCES

- Allison R. J., Goodwin S. P., Parker R. J., 2010, MNRAS, 407, 1098
- Allison R. J., Goodwin S. P., Parker R. J., de Grijs R., Portegies Zwart S. F., Kouwenhoven M. B. N., 2009a, ApJ, 700, L99
- Allison R. J., Goodwin S. P., Parker R. J., Portegies Zwart S. F., de Grijs R., Kouwenhoven M. B. N., 2009b, MNRAS, 395, 1449
- André P., Men’shchikov A., Bontemps S., Könyves V., Motte F., et al., 2010, A&A, 518, L102+
- Ascenso J., Alves J., Lago M. T. V. T., 2009, Ap&SS, 324, 113

- Bate M. R., 2009, MNRAS, 392, 590  
 Bonnell I. A., Bate M. R., Vine S. G., 2003, MNRAS, 343, 413  
 Bonnell I. A., Clark P., Bate M. R., 2008, MNRAS, 389, 1556  
 Bonnell I. A., Davies M. B., 1998, MNRAS, 295, 691  
 Bontemps S., André P., Könyves V., Men'shchikov A., Schneider N., et al., 2010, A&A, 518, L85+  
 Casertano S., Hut P., 1985, ApJ, 298, 80  
 Chen L., de Grijs R., Zhao J. L., 2007, AJ, 134, 1368  
 Hillenbrand L. A., Hartmann L. W., 1998, ApJ, 492, 540  
 Kirk H., Myers P. C., 2011, ApJ, 727, 64  
 Könyves V., André P., Men'shchikov A., Schneider N., Arzoumanian D., et al., 2010, A&A, 518, L106+  
 Maschberger T., Clarke C. J., Bonnell I. A., Kroupa P., 2010, MNRAS, 404, 1061  
 Moeckel N., Bonnell I. A., 2009, MNRAS, 400, 657  
 Parker R. J., Bouvier J., Goodwin S. P., Moraux E., Allison R. J., Guieu S., Güdel M., 2011, MNRAS, 51  
 Schmeja S., Kumar M. S. N., Ferreira B., 2008, MNRAS, 389, 1209  
 Stolte A., Brandner W., Brandl B., Zinnecker H., 2006, AJ, 132, 253  
 von Hoerner S., 1963, ZAp, 57, 47  
 Wang J., Townsley L. K., Feigelson E. D., Broos P. S., Getman K. V., Román-Zúñiga C. G., Lada E., 2008, ApJ, 675, 464  
 Zahn C. T., 1971, IEEE Transactions on Computers, 20, 68

This paper has been typeset from a  $\text{\TeX}/\text{\LaTeX}$  file prepared by the author.